

Supplemental Material

(I) MARTINI in CHARMM

In order to compute transitions faster and manage memory efficiently, the MARTINI force field originally implemented in GROMACS was ported in CHARMM. The original 4:1 mapping of atoms to beads and the parameter for each bead was preserved as in the MARTINI force field.

Angle potential

While the functional form of the bonded interaction is the same in both CHARMM and GROMACS, the functional form of the angle potential function in GROMACS (Equation 2) uses the cos angle term unlike CHARMM (Equation 1), where, K_θ is the bond angle constant, θ is the bond angle, θ_0 is the equilibrium bond angle. The difference in the angle potential function between GROMACS and CHARMM was addressed by adjusting the force constant to match the potential well for each angle in GROMACS. We use a modified force constant which corrects for the difference between the cos based and angles based terms. This can be calculated from Equation (3)

$$U = \sum_{bonds} \frac{1}{2} K_\theta (\theta - \theta_0)^2 \quad (1)$$

$$V_{angle} = \frac{1}{2} K_{angle} \{\cos(\theta) - \cos(\theta_0)\}^2 \quad (2)$$

$$X = \sum K_{GR}(\cos\theta - \cos\theta_o)^2 - K_{CH}(\theta - \theta_o)^2 \quad (3)$$

where K_{GR} and K_{CH} are the force constants in GROMACS and in CHARMM respectively.

For the angles 150 and 210, in the MARTINI force field, the barrier height is very low and therefore, beads with angles 150 or 210 can flip to either of the conformations easily (Figure S1). When the same force constant was used to define the angle potential in CHARMM, it resulted in a higher energy barrier. So, we worked out the correction in the force constants for angles 210 and 150 to represent the energy barrier better. The force constant for the 210 angle term was reduced from to 1.632 kcal/mol and for 150 it was reduced to 1.5347 kcal/mol. We have done least square error estimates for different force constants for both angles to choose the best force constant that represents the energy curve. We have also calculated the modified force constants for other side chain angles and used them in our parameter file (Table S1).

Side Chain Angles	K-GRO (kJ/mol)	K-CH (kcal/mol)	K-adjusted (kcal/mol)
90	50	5.98	4.61
150	50	5.98	2.10
180	25	2.99	1.47
210	50	5.98	2.09
100	25	2.99	2.22
BackBone angles			
127	25	2.99	2.48
96	700	83.65	60.47
134	25	2.99	2.32
100	25	2.99	2.22

Table S1: The backbone and side chain angles in MARTINI. K-GRO is the force constant in GROMACS. K-CH is the converted force constant in CHARMM. K-adjusted is the force constant adjusted to better fit the angle potential.

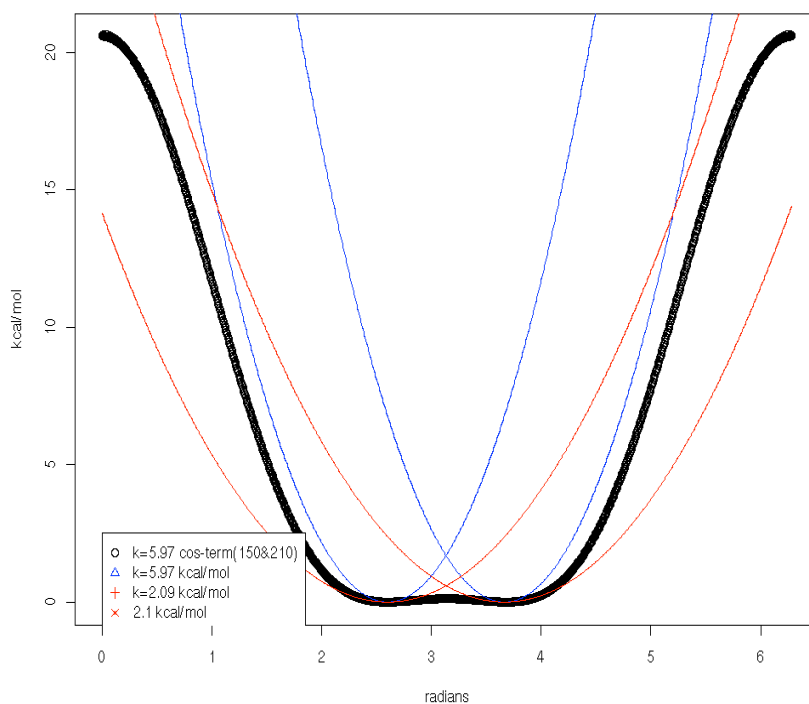


Figure S1: Angle potential functions. The GROMACS angle function for 150° and 210° (black) has a low barrier in the middle which enables the angles to flip from one conformation to another easily. The CHARMM potential for this angle (blue) with the MARTINI specified force constant produces a higher barrier. This was lowered by altering the force constant (red).

Non-bonded Terms

In the coarse grained parameters, for the non-bonded exclusion list, we have used the NBXMOD value as 2 (bonded interactions). This is to ensure proper interactions between only bonded beads since there is a 4:1 mapping of atoms in the MARTINI force field. A CUTNM of 15.0Å, CTOFNB of 12.0Å and CTONNB of 9.0Å was used. The dielectric constant was set to 15.0. We used the NBFIX set of parameters to specify individual bead type VDW pair interactions. For this reason, it also requires that CHARMM be recompiled to allow a higher number (1800) for NBFIX to be used.

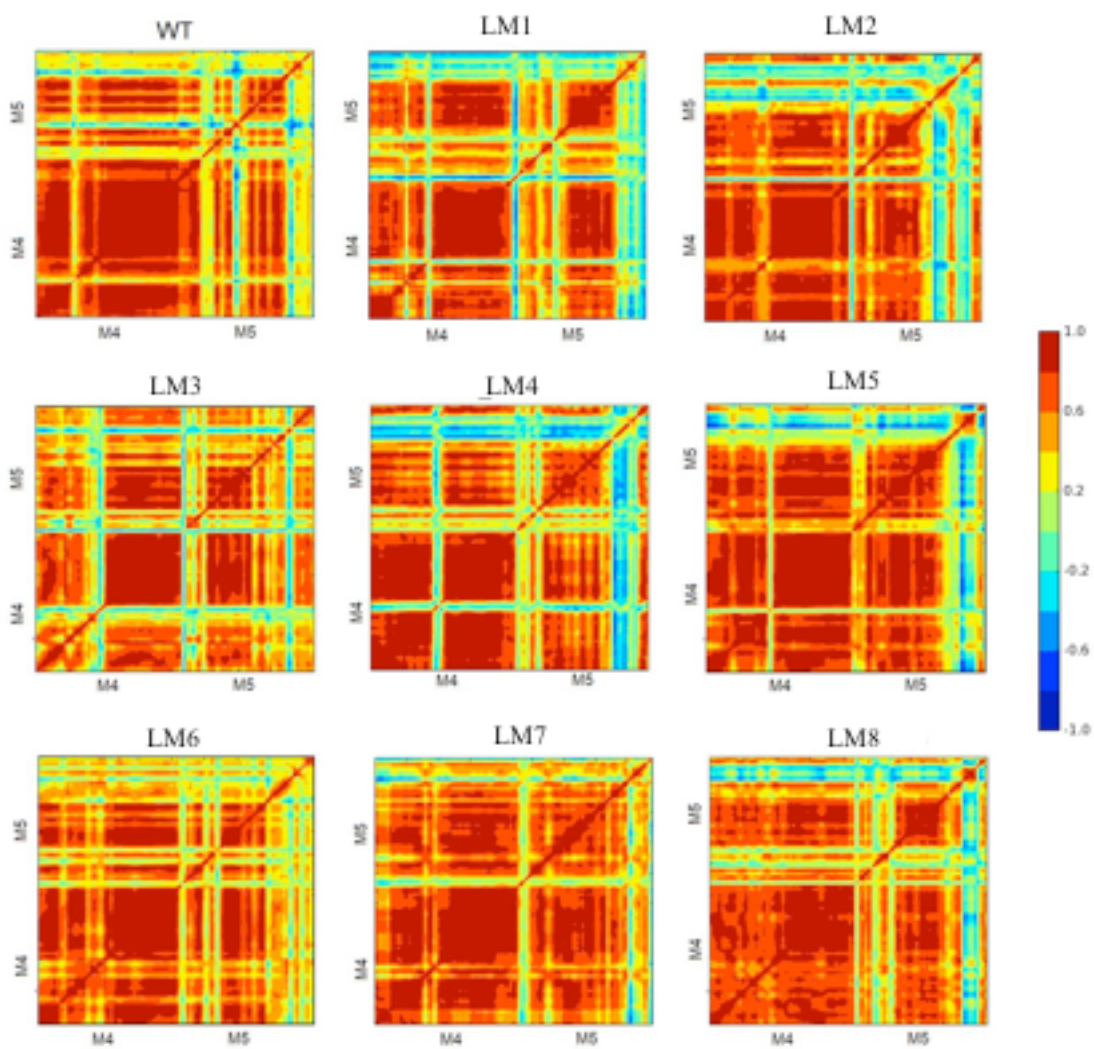


Figure S2: Two dimensional correlation maps for the M4 and M5 transmembrane helices in the WT and mutants. Color codes corresponding to the strength of the correlation is shown on the right.

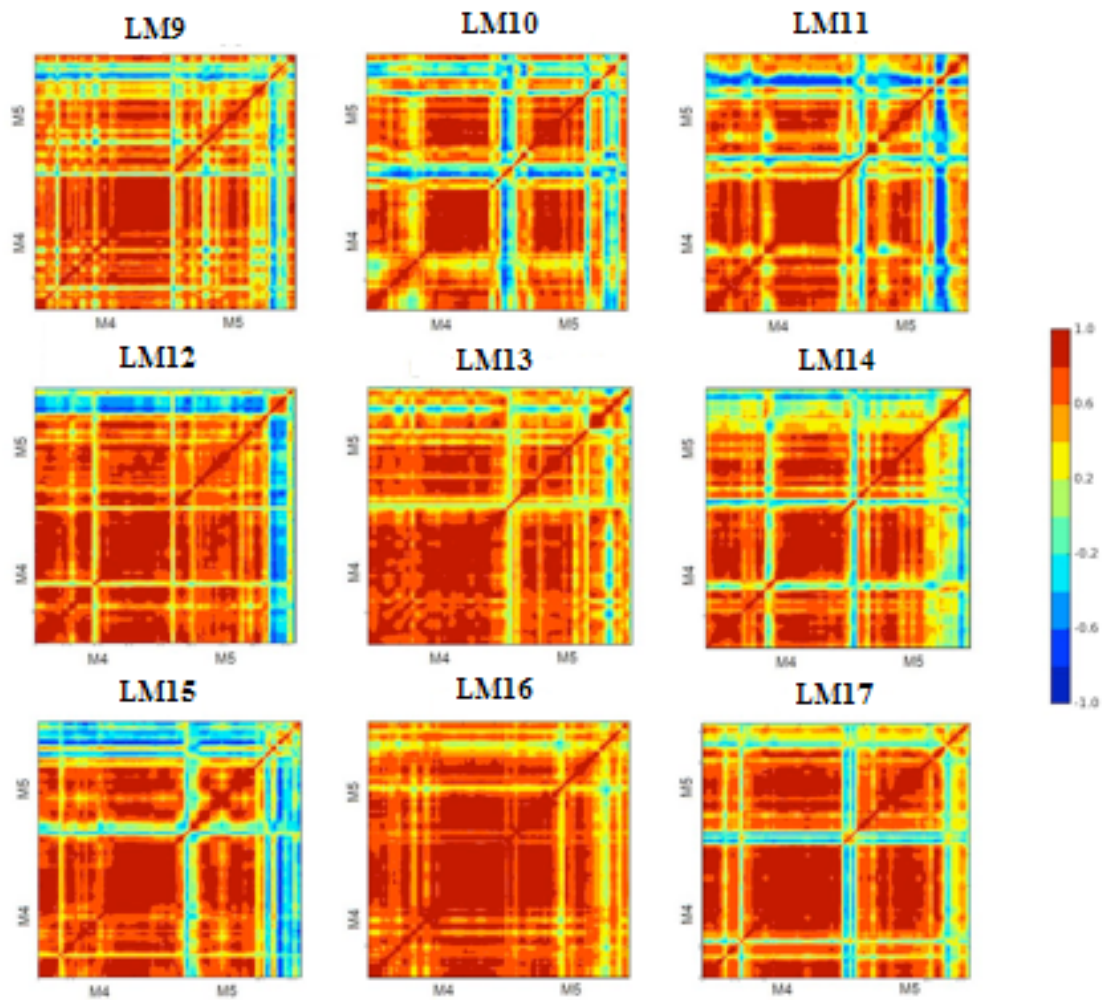


Figure S3: Two dimensional correlation maps for the M4 and M5 transmembrane helices in the mutants. Color codes corresponding to the strength of the correlation is shown on the right.

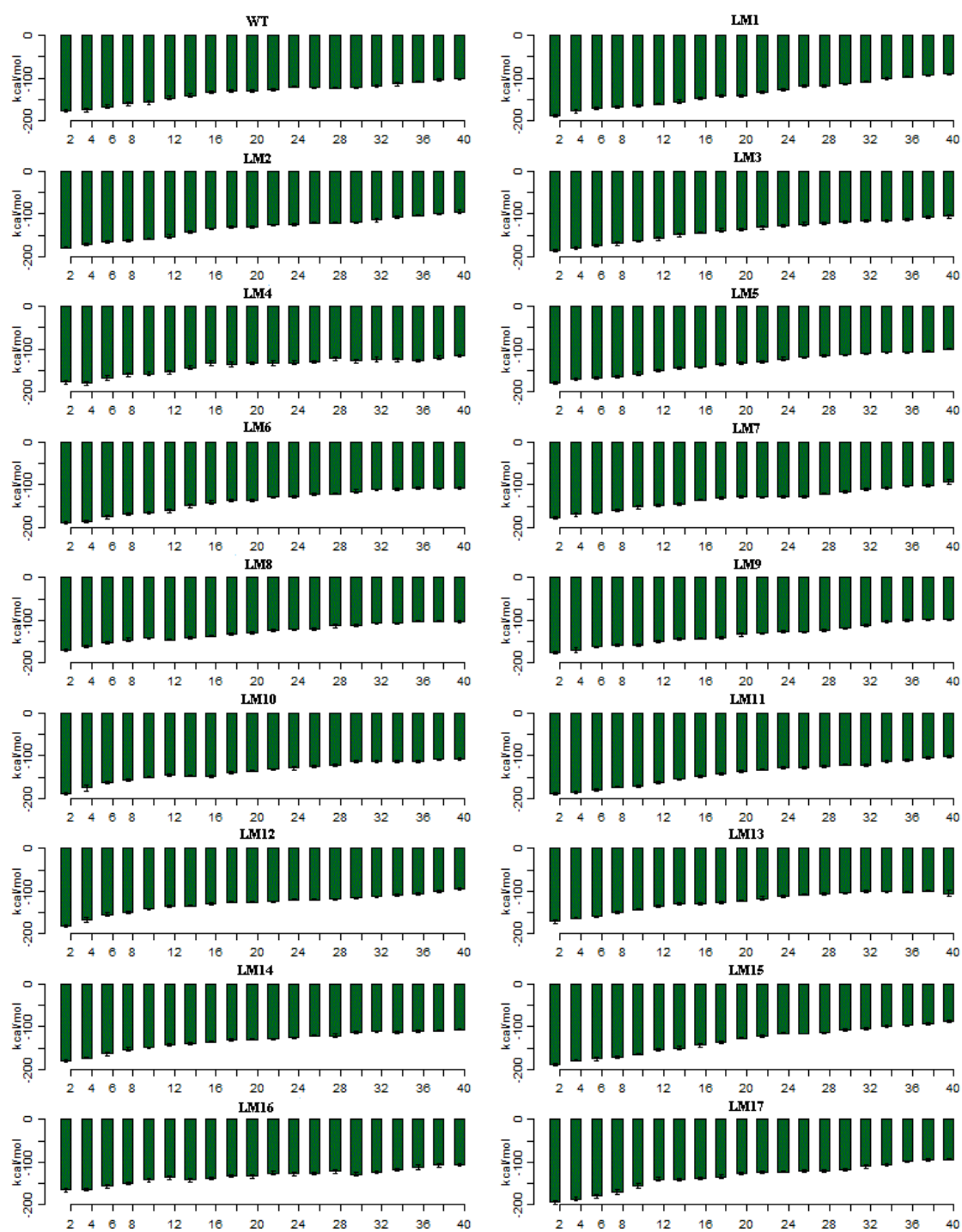


Figure S4: The interaction energy between the N-Domain and the P-domain during the E1P → E2P transition. The x-axis shows the progress of the transition from the starting state (2ZBD) to the ending state (1WPG). The transitions are divided into 5% percent completion bins and the values are averaged over 50 transitions for each mutant.

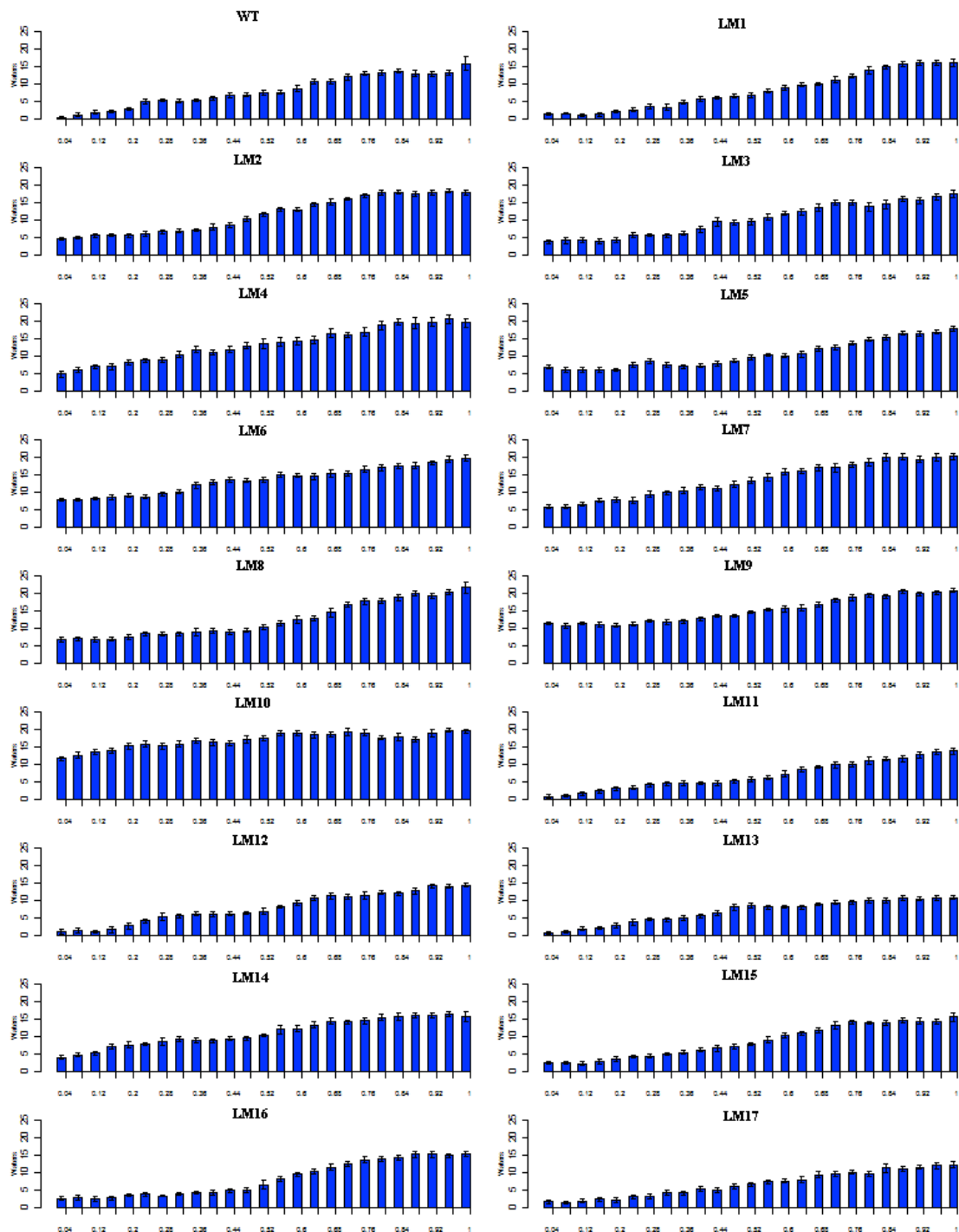


Figure S5: The number of waters within an 8Å radius of A3 helix and the the P-domain helices (P5, P6 and P7) during the E1P -> E2P transition. The x-axis shows the progress of the transition (0 -> 1) from the starting state (2ZBD) to the ending state (1WPG). The transitions are divided into 5% percent completion bins and the values are averaged over 50 transitions for each mutant.

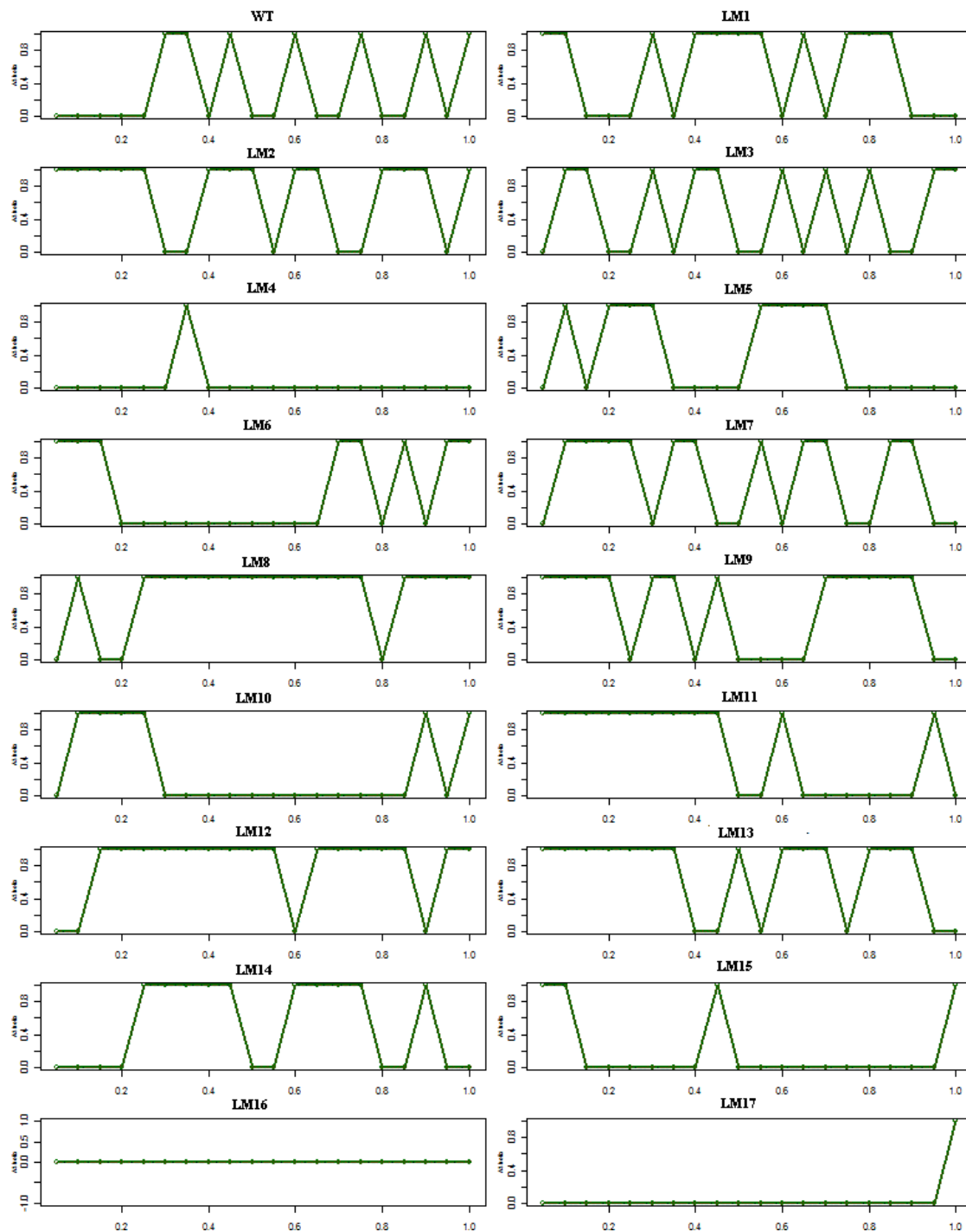


Figure S6: The formation of the A3 helix during the E1P \rightarrow E2P transition. The value on the y-axis indicates the formation of the A3 helix, zero represents the A3 region lacking secondary structure and 1 represents A3 region having a helical structure. The x-axis shows the progress of the transition (0 \rightarrow 1) from the starting state (2ZBD) to the ending state (1WPG). The transitions are divided into 5% percent completion bins and the values are averaged over 50 transitions for each mutant

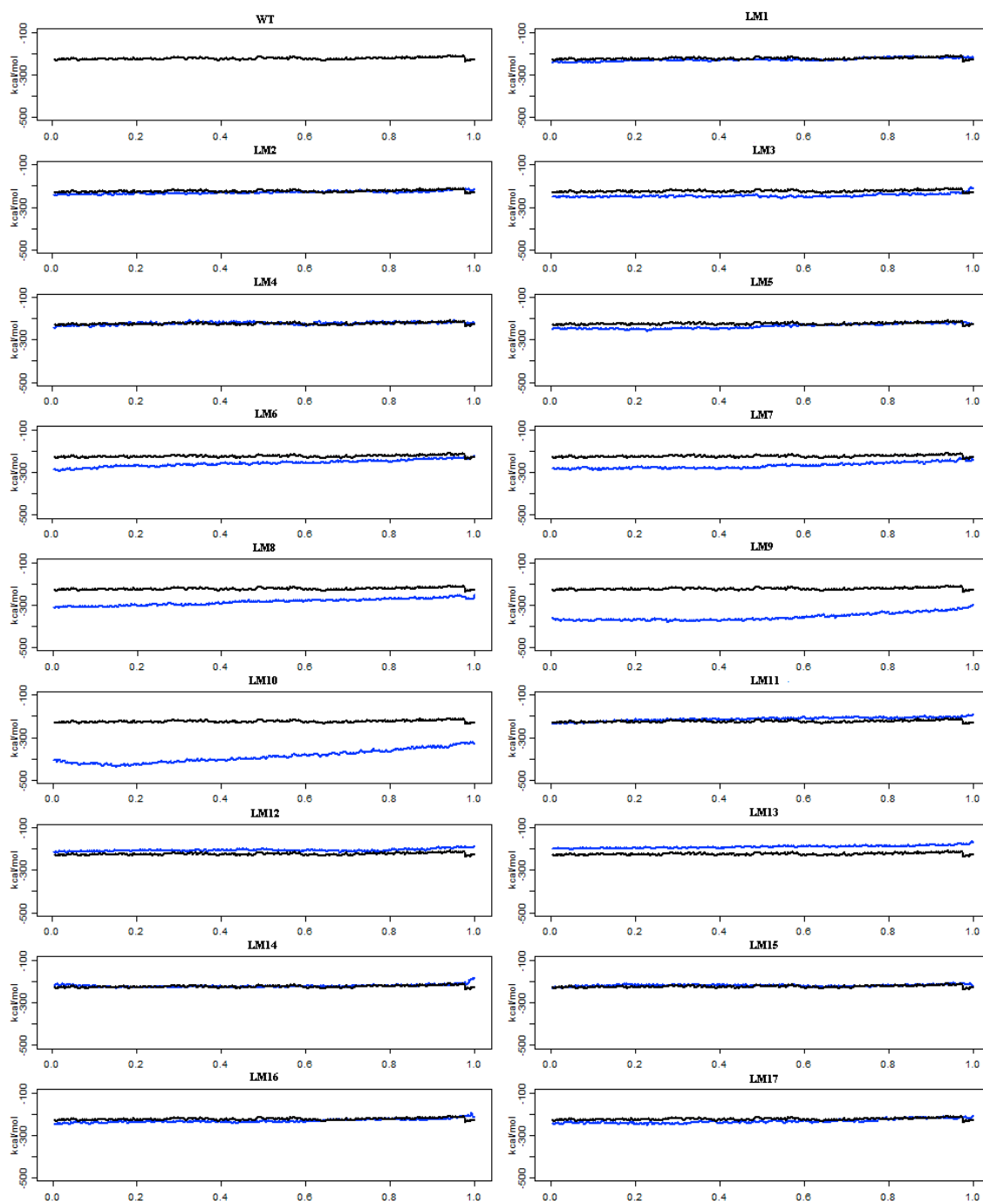


Figure S7: Interaction of waters with the M3-linker region during the E1P \rightarrow E2P transition for the various mutants. The first panel shows the interaction for the WT, in the subsequent panels, the mutants (blue) are compared with the WT (black)

Mutants	Estimated free energy (kcal/mol)
WT	-7188.91
LM1	-8227.26
LM2	-8090.31
LM3	-8657.05
LM4	-9231.53
LM5	-9436.22
LM6	-10154.5
LM7	-10306.14
LM8	-11799.28
LM9	-14896.58
LM10	-18282.01
LM11	-7457.19
LM12	-7296.59
LM13	-7357.34
LM14	-7463.92
LM15	-7307.59
LM16	-7775.31
LM17	-8928.82

Table S2: Estimated free energy values for the EIP state for the WT and all the mutants.